New Perspectives for QCD Physics at the LHC

STANLEY J. BRODSKY[*1]

1SLAC National Accelerator Laboratory
Stanford University, Stanford, California 94309
and CP3-Origins, Southern Denmark University
Odense, Denmark
[*]E-mail: sjbth@slac.stanford.edu

I review a number of topics where conventional wisdom relevant to hadron physics at the LHC has been challenged. For example, the initial-state and final-state interactions of the quarks and gluons entering perturbative QCD hard-scattering subprocesses lead to the breakdown of traditional concepts of factorization and universality for transverse-momentum-dependent observables at leading twist. These soft-gluon rescattering effects produce Bjorken-scaling single-spin asymmetries, the breakdown of the Lam-Tung leading-twist relation in Drell-Yan reactions, as well as diffractive deep inelastic scattering, The antishadowing of nuclear structure functions is predicted to depend on the flavor quantum numbers of each quark and antiquark, thus explaining the anomalous nuclear dependence observed in deep-inelastic neutrino scattering. Isolated hadrons can be produced at large transverse momentum directly within a hard higher-twist QCD subprocess, rather than from jet fragmentation, even at the LHC. Such "direct" processes can explain the observed deviations from pQCD predictions of the power-law fall-off of inclusive hadron cross sections at fixed $x_T = 2p_T/\sqrt{s}$, as well as the "baryon anomaly", the anomalously large proton-to-pion ratio seen in high-centrality heavy-ion collisions at RHIC. The intrinsic charm contribution to the proton structure function at high x can explain the large rate for high p_T photon plus charm-jet events observed by D0 at the Tevatron. The intrinsic charm and bottom distributions imply a large production rate for charm and bottom jets at high p_T at the LHC, as well as a novel mechanism for Higgs and Z^0 production at high x_F. The light-front wavefunctions derived in AdS/QCD can be used to calculate jet hadronization at the amplitude level. The elimination of the renormalization scale ambiguity for the QCD coupling using the scheme-independent BLM method will improve the precision of QCD predictions and thus increase the sensitivity of searches for new physics at the LHC. The implications of "in-hadron condensates" for the QCD contribution to the cosmological constant are also discussed.

I. INTRODUCTION

The LHC will provide a crucial testing ground for testing QCD, not only at unprecedented energies and momentum transfers, but also at extreme particle densities. In this contribution I will review a number of topics where unexpected new perspectives for QCD physics at the LHC have emerged.

1. *High Transverse Momentum Hadron Production via Direct Hard Subprocesses*
   It is natural to assume that high transverse momentum hadrons in inclusive high energy hadronic collisions, such as $pp \to HX$, can only arise from jet fragmentation. In fact, a significant fraction of high $p_\perp^H$ isolated hadrons can emerge directly from hard higher-twist subprocess [1, 2] even at the LHC. The direct production of hadrons can explain [3] the remarkable "baryon anomaly" observed at RHIC: the ratio of baryons to mesons at high $p_\perp^H$, as well as the power-law fall-off $1/p_\perp^n$ at fixed $x_\perp = 2p_\perp/\sqrt{s}$, both increase with centrality [4], opposite to the usual expectation that protons should suffer more energy loss in the nuclear medium than mesons.

A fundamental test of leading-twist QCD predictions in high transverse momentum hadronic reactions is the measurement of the power-law fall-off of the inclusive cross section [5] $E d\sigma/d^3p(AB \to CX) = F(\theta_{cm}, x_T)/p_T^{n_{eff}}$ at fixed $x_T = 2p_T/\sqrt{s}$ and fixed θ_{CM}, where $n_{eff} \sim 4 + \delta$. Here $\delta = \mathcal{O}(1)$ is the correction to the conformal prediction arising from the QCD running coupling and the DGLAP evolution of the input parton distribution and fragmentation functions [1, 2, 6]. The usual expectation is that leading-twist subprocesses will dominate measurements of high p_T hadron production at RHIC and Tevatron energies. In fact, the data for isolated photon production $pp \to \gamma_{\text{direct}} X$, as well as jet production, agrees well with the leading-twist scaling prediction $n_{eff} \simeq 4.5$ as shown in Fig.1 [1]. However, as seen in Fig.1, measurements of n_{eff} for hadron production are not consistent with the leading twist predictions. Striking deviations from the leading-twist predictions were also observed at lower energy at the ISR and Fermilab fixed-target experiments [5, 7, 8]. The high values n_{eff} with x_T seen in the data indicate the presence of an array of higher-twist processes, including subprocesses

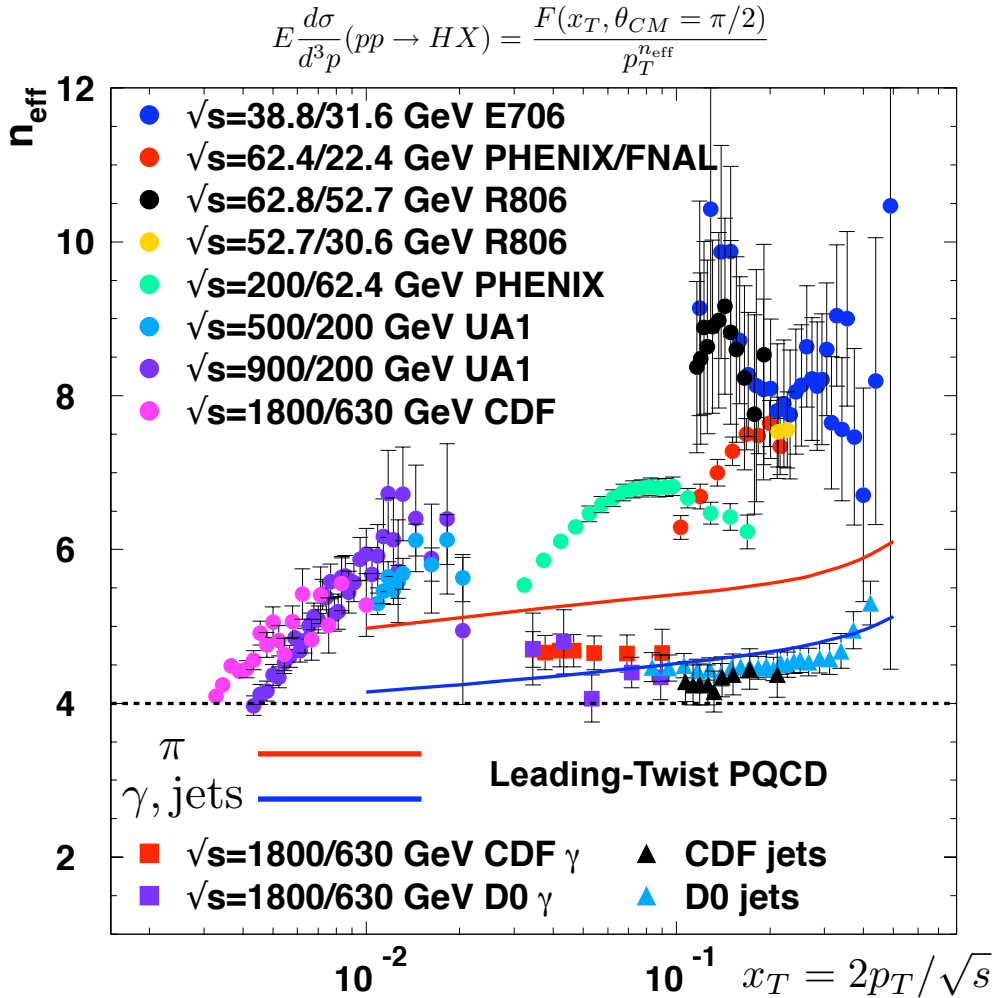$$E\frac{d\sigma}{d^3p}(pp \to HX) = \frac{F(x_T, \theta_{CM} = \pi/2)}{p_T^{n_{\mathrm{eff}}}}$$

FIG. 1: Comparison of RHIC and fixed-target data for hadron, isolated photon, and jet production with the leading-twist pQCD predictions for the power-law falloff of the semi-inclusive cross section $Ed\sigma/d^3p(pp \to HX) = F(x_T, \theta_{CM} = \pi/2)/p_T^{n_{\mathrm{eff}}}$ at fixed x_T. The data from R806, PHENIX, ISR/FNAL, E706 are for charged or neutral pion production, whereas the CDF, UA1 data at small x_T are for charged hadrons. The blue curve is the prediction of leading-twist QCD for isolated photon and jet production, including the scale-breaking effects of the running coupling and the evolution of the proton structure functions. The red curve is the QCD prediction for pion production, which also includes the effect from the evolution of the fragmentation function. The dashed line at $n_{\mathrm{eff}} = 4$ is the prediction of the scale-invariant parton model. From Arleo, et al. [1].

where the hadron enters directly, rather than through jet fragmentation [9]. The predicted deviations for the experimental and NLO scaling exponent at RHIC and the LHC with PHENIX preliminary measurements are shown in Fig. 2.

I will discuss further consequences of direct QCD production processes in section II.

2. *Breakdown of Perturbative QCD Factorization and Universality*

The effects of initial and final-state interactions of the quarks and gluons entering hard processes at the LHC are usually assumed to be of higher-twist origin and thus power-law suppressed. However, as emphasized by Collins and Qiu [10], the traditional factorization formalism of perturbative QCD fails in detail for transverse-momentum-dependent observables in hard inclusive reactions because of initial- and final-state gluonic interactions at leading twist.

It is now well-understood that the final-state gluonic interactions of the scattered quark in deep inelastic lepton scattering lead to a T-odd non-zero spin correlation of the plane of the lepton-quark scattering plane with the polarization of the target proton [11]. This leading-twist Bjorken-scaling "Sivers effect" is process-dependent
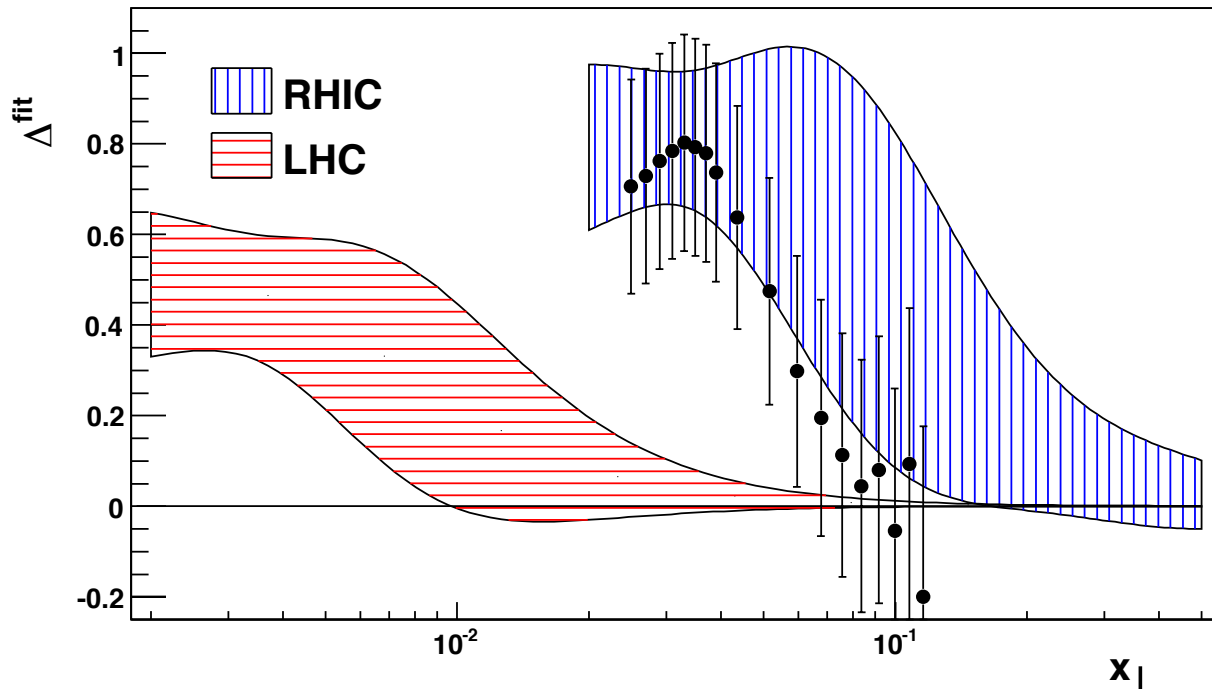
FIG. 2: Predicted difference Δ between the experimental and NLO scaling exponent at RHIC ($\sqrt{s} = 200, 500$ GeV) and the LHC ($\sqrt{s} = 7$ TeV as compared to $\sqrt{s} = 1.8$ TeV), compared to PHENIX preliminary measurements. From Arleo, et al. [1].

since QCD predicts an opposite-sign correlation [12, 13] in Drell-Yan reactions due to the initial-state interactions of the annihilating antiquark. The same final-state interactions of the struck quark with the spectators [14] also lead to diffractive events in deep inelastic scattering (DDIS) at leading twist, such as $\ell p \rightarrow \ell' p' X$, where the proton remains intact and isolated in rapidity; in fact, approximately 10% of the deep inelastic lepton-proton scattering events observed at HERA are diffractive [15, 16]. The presence of a rapidity gap between the target and the diffracted proton requires that the target remnant emerges in a color-singlet state; this is made possible in any gauge by the soft rescattering incorporated in the Wilson line or by augmented light-front wavefunctions [17].

In the case of hadron-hadron collisions, the quark and antiquark in the Drell-Yan subprocess $q\bar{q} \rightarrow \mu^+ \mu^-$ will interact with the spectators of the other hadron; this leads to an anomalous $\cos 2\phi \sin^2 \theta$ planar correlation in unpolarized Drell-Yan reactions [18]. This "double Boer-Mulders effect" can account for the large $\cos 2\phi$ correlation and the corresponding violation [18, 19] of the Lam Tung relation for Drell-Yan processes observed by the NA10 collaboration. Another important signal for factorization breakdown at the LHC will be the observation of a $\cos 2\phi$ planar correlation in dijet production.

It is usually assumed – following the intuition of the parton model – that the structure functions measured in deep inelastic scattering can be computed in the Bjorken-scaling leading-twist limit from the absolute square of the light-front wavefunctions, summed over all Fock states. In fact, the dynamical effects, such as the Sivers spin correlation and diffractive deep inelastic lepton scattering due to final-state gluon interactions, contribute to the experimentally observed DIS cross sections. Diffractive events also lead to the interference of two-step and one-step processes in nuclei which in turn, via the Gribov-Glauber theory, lead to the shadowing and the antishadowing of the deep inelastic nuclear structure functions [20]; such phenomena are not included in the light-front wavefunctions of the nuclear eigenstate. This leads to an important distinction between "dynamical" vs. "static" (wavefunction-specific) structure functions [21].

3. *Non-Universal Nuclear Distributions*

It is usually assumed that the nuclear modifications to the structure functions measured in deep inelastic lepton-nucleus and neutrino-nucleus interactions are identical; in fact, the Gribov-Glauber theory predicts that the antishadowing of nuclear structure functions is not universal, but depends on the quantum numbers of each struck quark and antiquark [20]. This observation can explain the recent analysis of Schienbein et al. [22] which shows that the NuTeV measurements of nuclear structure functions obtained from neutrino charged current
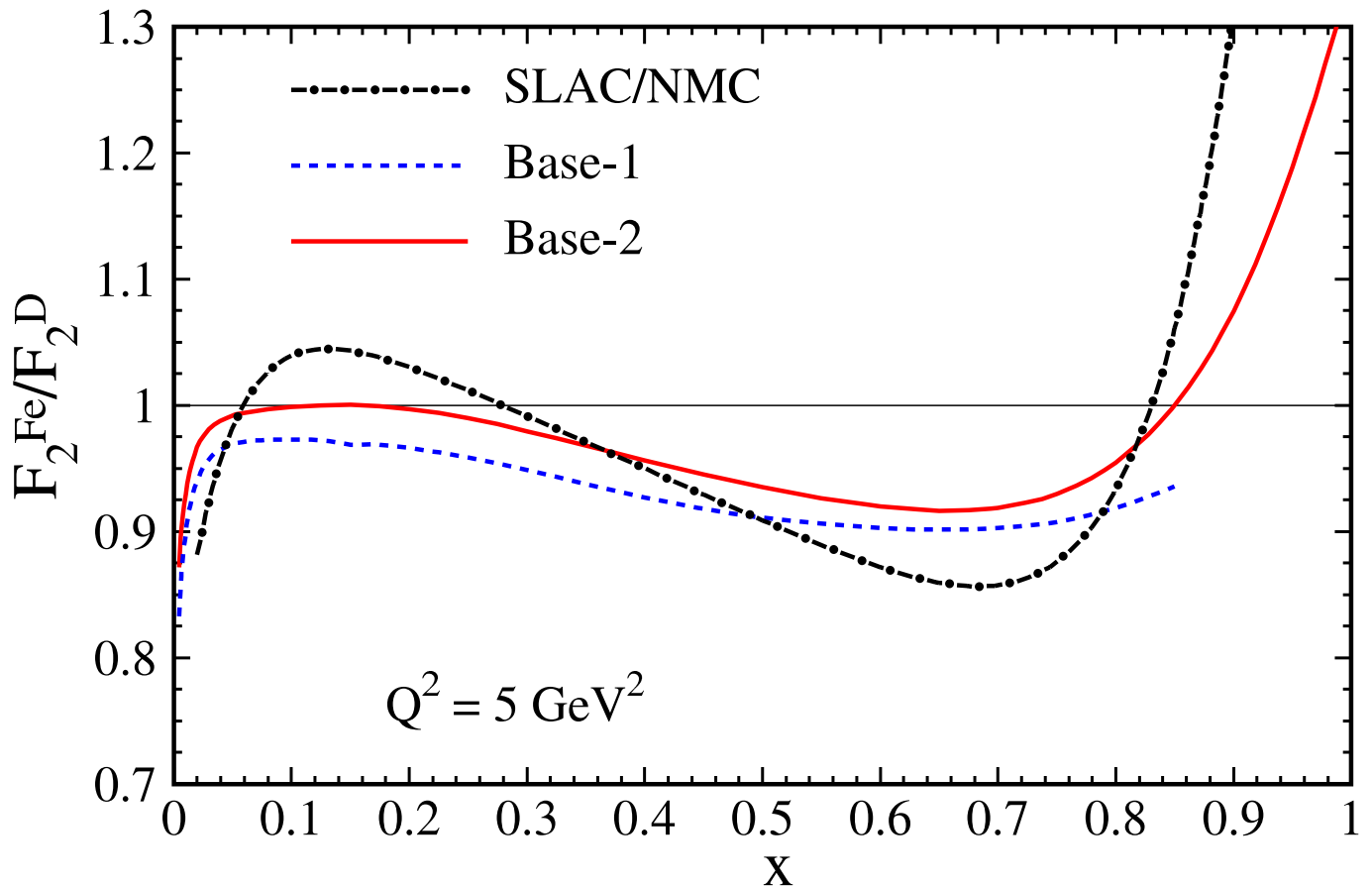
FIG. 3: Comparison of the (Iron to Deuteron) nuclear modification of SLAC/NMC neutral vs. NuTeV charged current (with range labeled by Base-1 and Base-2) deep inelastic structure functions at $Q^2 = 5$ GeV^2. From I. Schienbein et al. [22]

reactions differ significantly from the distributions measured in deep inelastic electron and muon scattering in the $0.1 < x < 0.2$ domain. See Fig. 3. I will discuss this in further detail in section IV.

4. *Intrinsic Heavy-Sea Quark Distributions*

Most parametrizations of the charm and bottom quark distributions in the proton structure functions only have support at low x since it is conventionally assumed that they only arise from gluon splitting $g \to Q\bar{Q}$. This erroneous assumption has led to many incorrect predictions; it is especially misleading for heavy hadron production at the LHC.

In fact, one can show from first principles that the proton light-front wavefunction contains *ab initio* intrinsic heavy quark Fock state components such as $|uudc\bar{c}>$ [23–26]. In contrast to the usual "extrinsic" contribution from gluon-splitting (i.e, DGLAP evolution), the intrinsic contributions are connected by gluons to at least two of the valence quarks of the proton. The intrinsic heavy quarks carry most of the proton's light-cone momentum since this minimizes the off-shellness of the Fock state. One can also associate the $|uudc\bar{c}>$ Fock state with meson-baryon fluctuations such as $|D(\bar{c}u)\Lambda_c(cud)>$. Thus, as is the case for intrinsic strangeness, the charm and anti-charm quarks can have different momentum and spin distributions [27].

The probability of the intrinsic component falls as $1/M_{Q\bar{Q}}^2$ due to the non-Abelian QCD couplings of the gluons [24, 26]. The heavy-quark pair $Q\bar{Q}$ in the intrinsic Fock state is thus primarily a color-octet, and the ratio of intrinsic charm to intrinsic bottom scales scales as $m_c^2/m_b^2 \simeq 1/10$, as can be verified from the operator product expansion in non-Abelian QCD [24, 26].

Intrinsic charm and bottom explain the origin of high x_F open-charm and open-bottom hadron production, as well as the single and double J/ψ hadroproduction cross sections observed at high x_F. The factorization-breaking nuclear $A^\alpha(x_F)$ dependence of hadronic J/ψ production cross sections is also explained. Kopeliovich, Schmidt, Soffer, Goldhaber, and I [28] have proposed a novel mechanism utilizing intrinsic heavy quarks for both

diffractive $pp \to pHp$ and inclusive Higgs production $pp \to HX$ in which the Higgs boson carries a significant fraction of the projectile proton momentum. The production mechanism is based on the subprocess $(Q\bar{Q})g \to H$ where the $Q\bar{Q}$ in the $|uudQ\bar{Q}>$ intrinsic heavy quark Fock state of the colliding proton has approximately 80% of the projectile protons momentum. I discuss this in further detail in section VI.

5. *Eliminating the Renormalization Scale Ambiguity*
It is often stated that the renormalization scale of the QCD running coupling $\alpha_s(\mu_R^2)$ cannot be fixed, and thus it has to be chosen in an *ad hoc* fashion. This statement is clearly false. For example, in QED the renormalization scale is simply the photon virtuality q^2 in the conventional Gell-Mann Low scheme since this sums all vacuum polarization corrections to all orders. In fact, as in QED, the renormalization scale for perturbative QCD can be fixed unambiguously in any scheme by shifting μ_R so that all terms associated with the QCD β function vanish. In general, each set of skeleton diagrams has its respective scale. The result is independent of the choice of the initial renormalization scale μ_{R0} as well as the scheme, thus satisfying the Callan-Symanzik equation and renormalization group invariance.

The conventional procedure where one guesses the renormalization scale, such as $\mu_R^2 = p_T^2$ and a range such as $1/2p_T^2 < \mu_R^2 < 2p_T^2$ is clearly problematic since it depends on the choice of renormalization scheme. This heuristic choice and range is wrong for the simplest example in QED, $e\mu \to e\mu$ scattering, since the exact answer which sums all vacuum contributions to all orders has the scale $\mu_R^2 = t$ in the Gell-Mann Low scheme [or $\mu_R^2 \simeq e^{-5/3}t$ in $\overline{MS}$ scheme [29]]; in fact, the exact resummed answer at forward CM angles always lies outside the guessed heuristic range. In other cases, the choice of a heuristic scale leads to nonsensical physical results [30] or even negative cross sections at NLO [31].

Clearly the elimination of the renormalization scale ambiguity would greatly improve the precision of QCD predictions and increase the sensitivity of searches for new physics at the LHC. Further discussion of the renormalization scale setting problem is given in Section III.

6. *QCD Condensates*
It is conventionally assumed that the vacuum of QCD contains quark $<0|q\bar{q}|0>$ and gluon $<0|G^{\mu\nu}G_{\mu\nu}|0>$ vacuum condensates, although the resulting vacuum energy density leads to a 10^{45} order-of-magnitude discrepancy with the measured cosmological constant. [32] However, a new perspective has emerged from Bethe-Salpeter and light-front analyses where the QCD condensates are identified as "in-hadron" condensates, rather than vacuum entities; the Gell-Mann-Oakes-Renner relation is still satisfied [33]. The "in-hadron" condensates become realized as higher Fock states of the hadron when the theory is quantized at fixed light-front time $\tau = x^0 + x^3/c$. I discuss this in further detail in section VII.

7. *Hidden Color*
In nuclear physics nuclei are composites of nucleons. However, QCD provides a new perspective: [34, 35] six quarks in the fundamental 3_C representation of $SU(3)$ color can combine into five different color-singlet combinations, only one of which corresponds to a proton and neutron. The deuteron wavefunction is a proton-neutron bound state at large distances, but as the quark separation becomes smaller, QCD evolution due to gluon exchange introduces four other "hidden color" states into the deuteron wavefunction [36]. The normalization of the deuteron form factor observed at large Q^2 [37], as well as the presence of two mass scales in the scaling behavior of the reduced deuteron form factor [34], suggest sizable hidden-color Fock state contributions in the deuteron wavefunction [38]. Hidden color can also play an important role in nuclear collisions involving quark distributions at high x_F.

8. *Light-Front Holography and Hadronization at the Amplitude Level*
A long-sought goal in hadron physics is to find a simple analytic first approximation to QCD analogous to the Schrödinger-Coulomb equation of atomic physics. This problem is particularly challenging since the formalism must be relativistic, color-confining, and consistent with chiral symmetry. de Teramond and I have shown that the correspondence between theories in a positive dilaton-modified five-dimensional anti-de Sitter space and confining field theories in physical space-time, leads to a simple Schrödinger-like light-front wave equation and a remarkable one-parameter description of nonperturbative hadron dynamics [39–41]. The model predicts a zero-mass pion for zero-mass quarks and a Regge spectrum of linear trajectories with the same slope in the (leading) orbital angular momentum L of the hadrons and their radial quantum number N.

"Light-Front Holography" [40] allows one to map the amplitudes $\phi(z)$ in AdS space directly to the light-front wavefunctions defined at fixed light-front time in 3+1 space. The resulting Lorentz-invariant relativistic light-front wave equations are functions of an invariant impact variable ζ which measures the separation of the quark and gluonic constituents within the hadron at equal light-front time. This correspondence was derived by
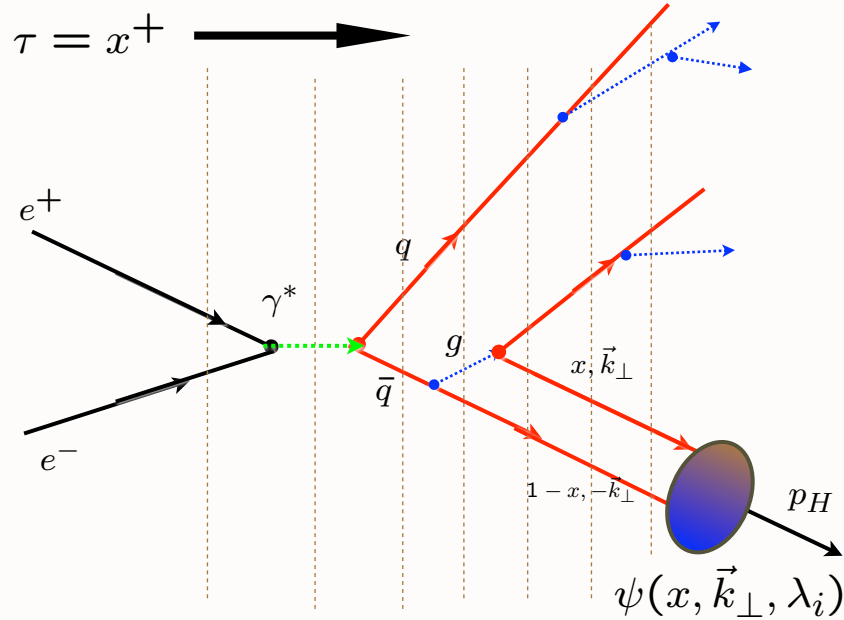
FIG. 4: Hadronization at the amplitude level. The off-shell T-matrix is computed in light-front Hamiltonian perturbation theory, evolving in light-front time $\tau = t + z/c$. The hadronic light-front wavefunctions convert the off-shell quarks and gluons to on-shell hadrons.

showing that the Polchinski-Strassler formula [42] for form factors in AdS space is equivalent to the Drell-Yan West light-front matrix element both for external electromagnetic and gravitational currents. One then finds an exact mapping between z in AdS space and the invariant impact separation ζ in 3+1 space-time. In the case of two-parton wavefunctions, one has $\zeta = \sqrt{x(1-x)b_\perp^2}$, where $b_\perp$ is the usual impact separation conjugate to $k_\perp$ and $x = k^+/P^+$ is the light-front fraction. This correspondence agrees with the intuition that z is related inversely to the internal relative momentum, but the relation $z \to \zeta$ is precise and exact. This relation also provides a direct connection between light-front Hamiltonian equations for bound state systems and the AdS wave equations. One thus obtains a semi-classical frame-independent first approximation to the spectra and light-front wavefunctions of meson and baryon light-quark bound states, which in turn predicts the behavior of the pion and nucleon form factors. The theory implements chiral symmetry in a novel way: the effects of chiral symmetry breaking increase as one goes toward large interquark separation. The the hadron eigenstates generally have components with different orbital angular momentum; e.g., the proton eigenstate in AdS/QCD with massless quarks has $L = 0$ and $L = 1$ light-front Fock components with equal probability. The AdS/QCD soft-wall model also predicts the form of the non-perturbative effective coupling $\alpha_s^{AdS}(Q)$ and its β-function [43].

The AdS/QCD light-front wavefunctions obtained from AdS/QCD and Light-Front Holography provide a method for computing the hadronization of quark and gluon jets at the amplitude level [44]. This is illustrated for $e^+ e^- \to \gamma^* \to$ hadrons in Fig. 4. An analogous method was used for QED to predict the production of relativistic antihydrogen [45].

II. DIRECT QCD PRODUCTION PROCESSES AT THE LHC

It should be emphasized that the existence of dynamical higher-twist processes in which a hadron interacts directly within a hard subprocess is a prediction of QCD. For example, the subprocess $\gamma^* q \to \pi q$, where the pion is produced directly through the pion's $\bar{q}q \to \pi$ distribution amplitude $\phi_\pi(x, Q)$ underlies deeply virtual meson scattering $\gamma p \to \pi X$. The corresponding timelike subprocess $\pi q \to \gamma^* q$ dominates the Drell-Yan reaction $\pi p \to \ell^+ \ell^- X$ at high x_F [46], thus accounting for the change in angular distribution from the canonical $1 + \cos^2 \theta$ distribution, for transversely polarized virtual photons, to $\sin^2 \theta$, corresponding to longitudinal photons; the virtual photon thus becomes longitudinally polarized at high x_F, reflecting the spin of the pion entering the direct QCD hard subprocess. Crossing predicts reactions where the final-state hadron appears directly in the subprocess such as $e^+ e^- \to \pi X$ at $z = 1$. The nominal power-law fall-off at fixed x_T is set by the number of elementary fields entering the hard subprocess $n_{\rm eff} = 2n_{\rm active} - 4$. The power-law fall-off $(1 - x_T)^F$ at high x_T is set by the total number of spectators $F = 2n_{\rm spectators} - 1$ [9], up to spin corrections.

The direct higher-twist subprocesses, where the trigger hadron is produced within the hard subprocess avoid the waste of same-side energy, thus allowing the target and projectile structure functions to be evaluated at the minimum values of x_1 and x_2 where they are at their maximum. Examples of direct baryon and meson higher-twist subprocesses are: $ud \to \Lambda \bar{s}, u\bar{d} \to \pi^+ g, ug \to \pi^+ d, u\bar{s} \to K^+ g, ug \to K^+ s$. These direct subprocesses involve the distribution amplitude of the hadron which has dimension Λ_{QCD} for mesons and Λ_{QCD}^2 for baryons; thus these higher-twist contributions to the inclusive cross section $E d\sigma/d^3 p$ at fixed x_T nominally scale as Λ_{QCD}^2/p_T^6 for mesons and Λ_{QCD}^4/p_T^8 for baryons.
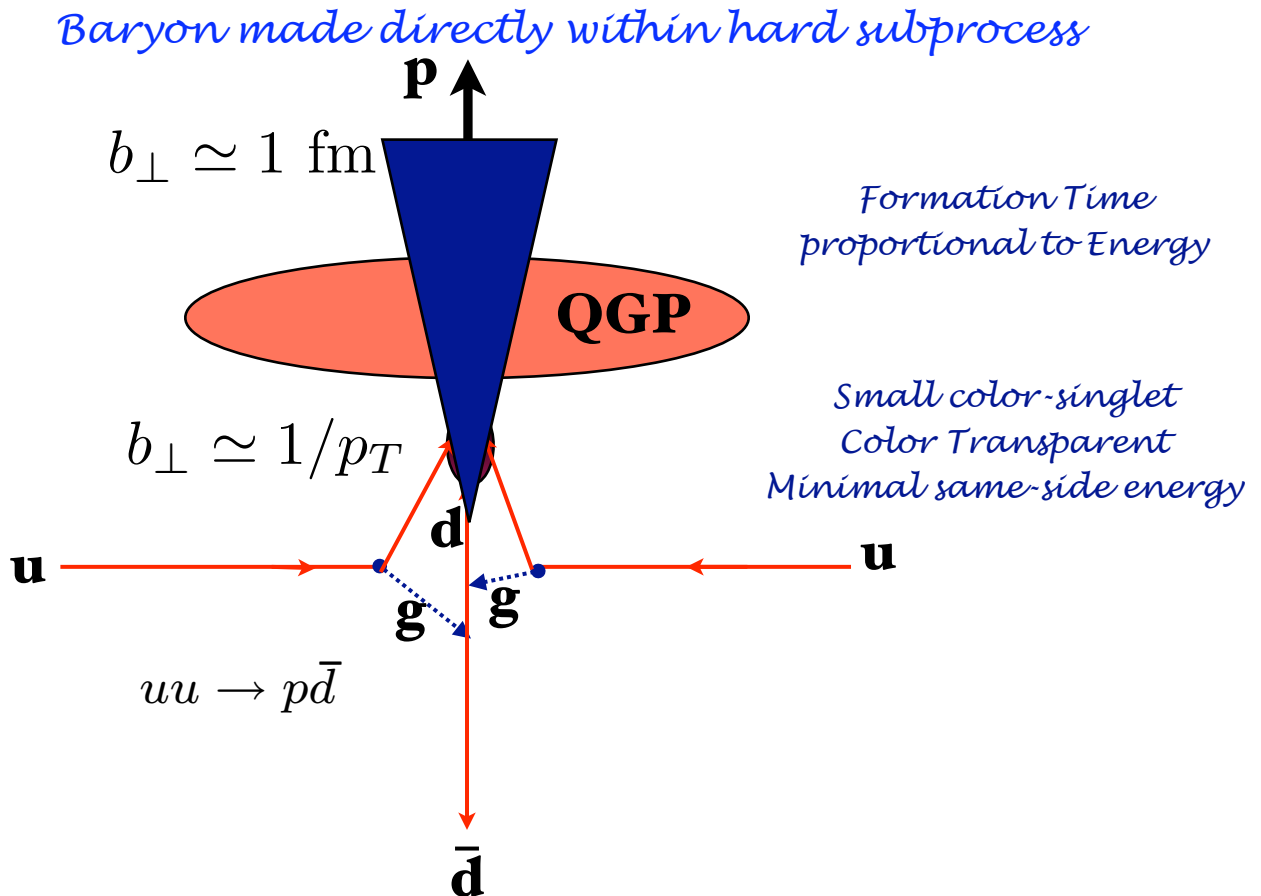

FIG. 5: Direct production of a proton in QCD. The proton is initially produced as a color-transparent small-size color singlet hadron.
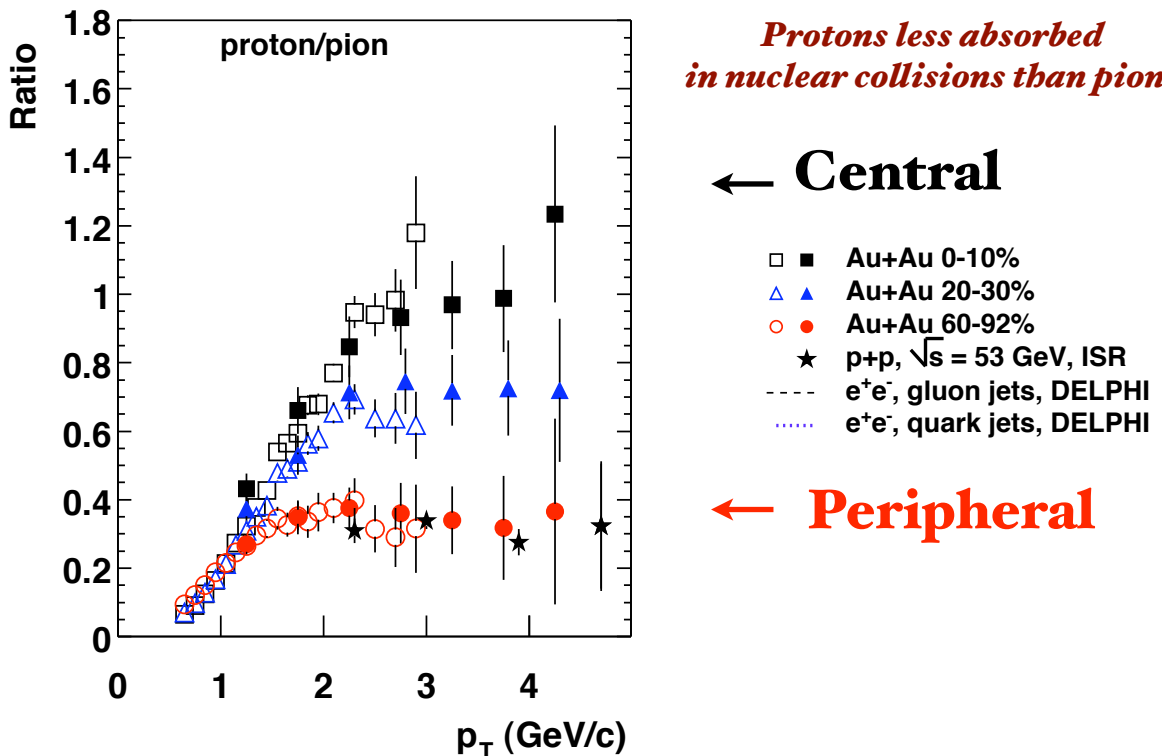
FIG. 6: The baryon anomaly observed by the PHENIX experiment at RHIC [4], The anomalous rise of the proton to pion ratio with centrality at large p_T.

The behavior of the single-particle inclusive cross section will be a key test of QCD at the LHC, since the leading-twist prediction for n_{eff} is independent of the detailed form of the structure and fragmentation functions. The fixed-x_T scaling of the proton production cross section $Ed\sigma/d^3p(pp \to pX)$ is particularly anomalous, far from the $1/p_T^4$ to $1/p_T^5$ scaling predicted by pQCD [6]. See Fig. 1. Sickles and I [47] have argued that the anomalous features of inclusive high p_T proton production is due to hard subprocesses [6] where the proton is created directly within the hard reaction, such as $uu \to p\bar{d}$, such as the mechanism illustrated in Fig. 5. The fragmentation of a gluon or quark jet to a proton requires that the underlying 2 to 2 subprocess occurs at a higher transverse momentum than the p_T of the observed proton because of the fast-falling quark-to-proton fragmentation function $D_{q\to p}(z) \sim (1-z)^3$ at high momentum fraction z; in contrast, the direct subprocess is maximally energy efficient. Such "direct" reactions thus can explain the fast-falling power-law falloff observed at fixed x_T and fixed-θ_{cm} at the ISR, FermiLab and RHIC [6].

Since the proton is initially produced as a small-size $b_\perp \sim 1/p_T$ color-singlet state, it is "color transparent" [48], and it can thus propagate through dense nuclear matter with minimal energy loss. In contrast, the pions which are produced from jet fragmentation have a normal inelastic cross section. This provides an explanation [3] of the RHIC data [4], which shows a dramatic rise of the p to π ratio with increasing p_T when one compares peripheral with central heavy ion collisions, as illustrated in Fig. 6. The color transparency of the proton produced in the direct process also can explain why the index n_{eff} rises with centrality, as seen in Fig. 7, – the higher-twist color-transparent subprocess dominates in the nuclear medium [6]. In addition, the fact that the proton tends to be produced alone in a direct subprocess explains why the yield of same-side hadrons along the proton trigger is diminished with increasing centrality. Thus the QCD color transparency of directly produced baryons can explain the "baryon anomaly" seen in heavy-ion collisions at RHIC: the color-transparent proton state is not absorbed, but a pion produced from fragmentation is diminished in the nuclear medium [47]. The increase of n_{eff} with centrality is consistent with the nuclear survival
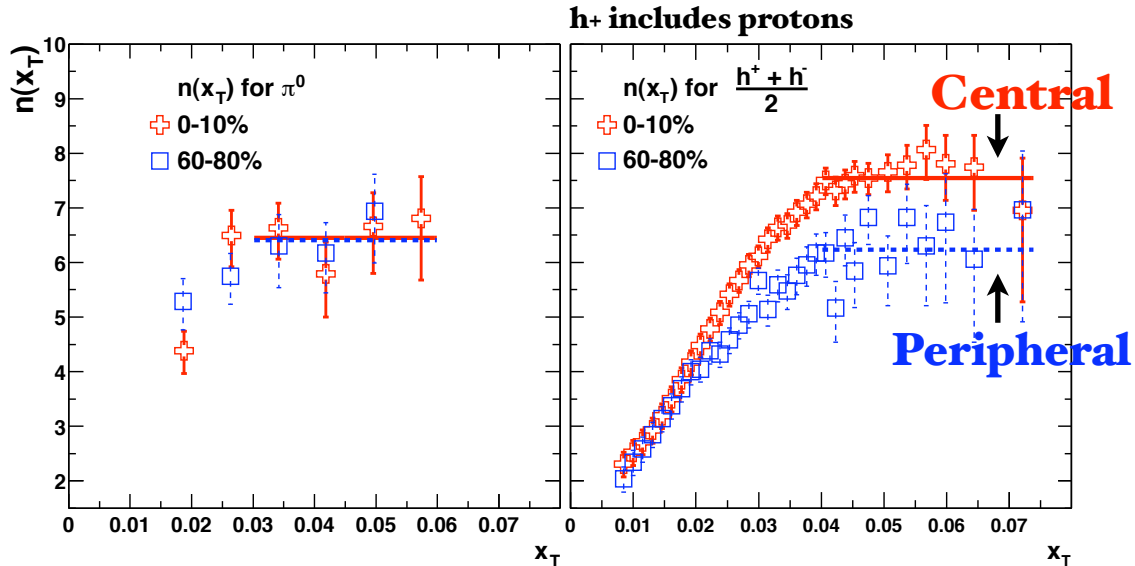
FIG. 7: The power-law scaling index n_{eff} at fixed $x_T = \frac{2p_T}{\sqrt{s}}$ as a function of centrality versus peripheral collisions, using spectra at $\sqrt{s} = 130$ GeV and $\sqrt{s} = 200$ GeV [47]. The positive-charged hadron trigger is dominated by protons at high p_T for central collisions, consistent with the color transparency of direct higher-twist baryon production processes.

of direct higher-twist subprocesses for both protons and antiprotons, and to a lesser extent, for mesons.

III.   ELIMINATION OF THE RENORMALIZATION SCALE AMBIGUITY - THE BLM METHOD

In the BLM method [49], the QCD scale μ_R is chosen, just as in QED, such that in principle all of the terms associated with the β function are summed into the QCD coupling [50] Quark loops can be used to identify the β terms, at least to two loops The remaining terms are identical to that of a conformal theory. Unlike heuristic scale-setting procedures, the BLM method gives results which are independent of the choice of renormalization scheme, as required by the transitivity property of the renormalization group. The divergent renormalon terms of order $\alpha_s^n \beta_0^n n!$ are transferred to the physics of the running coupling. Furthermore, one retains sensitivity to "conformal" effects which arise in higher orders, physical effects which are not associated with QCD renormalization. In contrast, the factorization scale μ_{fac} which sets the separation between nonperturbative dynamics of hadrons and the perturbative evolution of their parton distribution functions is arbitrary; it is unrelated to the factorization scale μ_R since it is present even in a conformal theory.

The BLM method also provides scale-fixed, scheme-independent connections between observables, such as the "Generalized Crewther Relation" [51, 52], in which Crewther's conformal prediction [53, 54] between the Bjorken sum rule and the annihilation cross section is effectively restored, as well as other "Commensurate Scale Relations" [55, 56]. The ratio of scales in the two observables is scheme-independent and ensures that the same number of quark
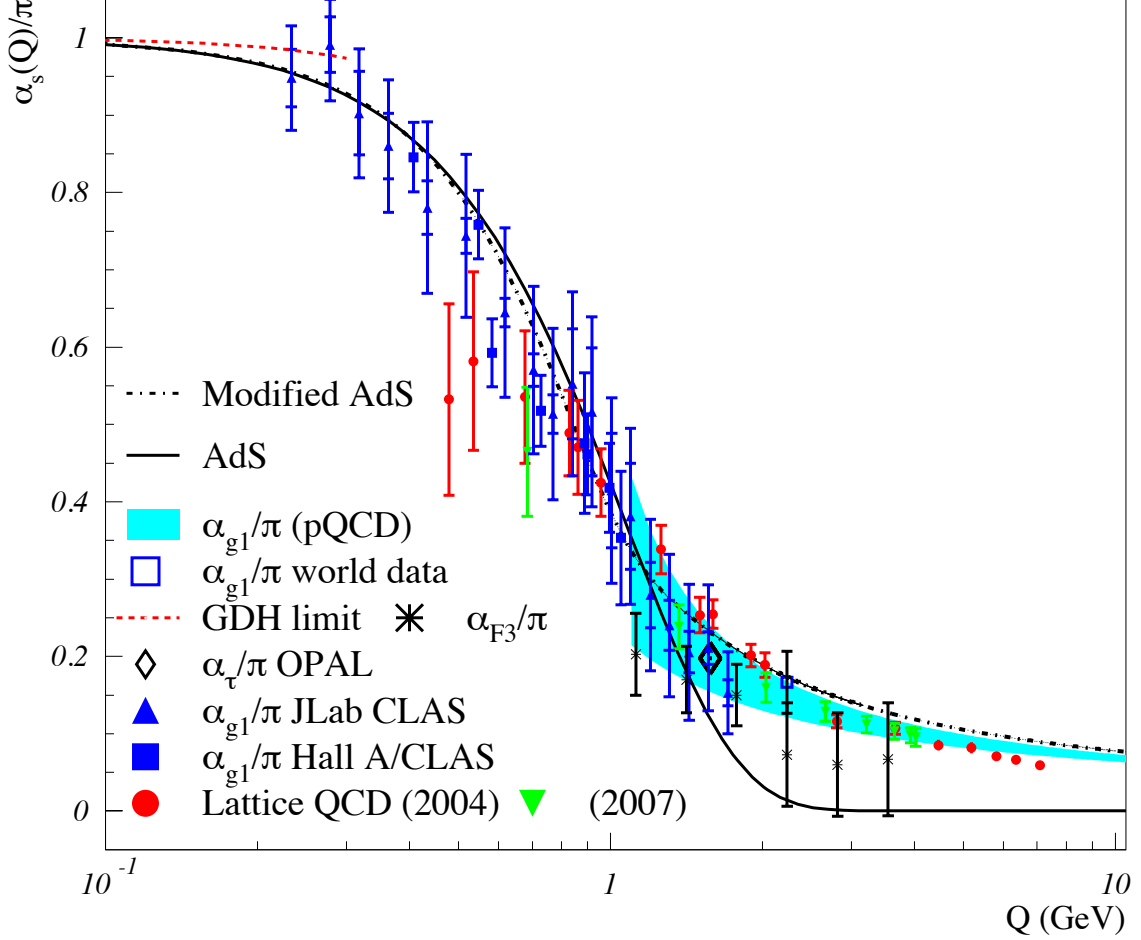
FIG. 8: The effective coupling $\alpha_s(Q^2) \propto e^{-\kappa^2 Q^2}$ predicted by light-front holographic mapping for $\kappa = 0.54$ GeV is compared with effective QCD couplings extracted from different observables and lattice results. Details on the comparison with other effective charges are given in Ref. [43].

flavors are active. Such relations between observables provide high precision test of QCD. The BLM method was used in Ref. [57] to unambiguously fix the pomeron intercept predicted by the BFKL analysis. The BLM method is also correct in the Abelian limit $N_C \to 0$ at fixed $\alpha = C_F \alpha_s$ [58], where $C_F = (N_C^2 - 1)/2N_C$ is the Casimir constant for $SU(N_C)$.

The consistent application of the BLM method to pQCD leads in most cases to multiple renormalization scales associated with different skeleton diagrams; for example in electron-electron scattering in QED there are separate scales $\alpha(t)$ and $\alpha(u)$ for photon exchange in the t and u-channels respectively. In the case of $e^+e^- \to e^+e^-$, the renormalization scales are $\mu_R^2 = t$ and $\mu_R^2 = s$ where $\alpha(s)$ is complex.

The scale controlling the three gluon coupling in QCD is particularly interesting. In the case of LHC processes such as $pp \to Q\bar{Q}X$, where the 3-gluon coupling enters at very different gluon virtualities, the BLM scale can be shown to be proportional to $q_1^2 q_2^2/q_3^2$ where q_3^2 is the largest of the gluon virtualities [59, 60]. This scale controls the onset of the new quark flavors that enter the triangle graph.

Thus, in many cases, the actual renormalization scale is much smaller than the largest hard scale in the process. Two distinctly different scales arise in heavy quark production at threshold: the relative momentum of the quarks governing the soft gluon exchange responsible for the Coulomb potential, and a large momentum scale approximately

equal to twice the quark mass for the corrections induced by transverse gluons [61].

Since one probes the QCD coupling at small virtuality even at the LHC, it is imperative to have good control on the QCD coupling in the soft domain. It is usually assumed that the QCD coupling $\alpha_s(Q^2)$ diverges at $Q^2 = 0$; i.e., "infrared slavery". In fact, determinations from lattice gauge theory, Bethe-Salpeter methods, effective charge measurements, gluon mass phenomena, and AdS/QCD all lead (in their respective schemes) to a finite value of the QCD coupling in the infrared [43]. Because of color confinement, the quark and gluon propagators vanish at long wavelength: $k < \Lambda_{QCD}$, and consequently, the quantum-loop corrections underlying the QCD β-function – decouple in the infrared, and the coupling freezes to a finite value at $Q^2 \to 0$ [62, 63]. See Fig. 8. This observation underlies the use of conformal methods in AdS/QCD.

Clearly the application of the BLM method to eliminate of the renormalization scale ambiguity would greatly improve the precision of QCD predictions and increase the sensitivity of searches for new physics at the LHC.

IV. LEADING-TWIST SHADOWING AND ANTI-SHADOWING OF NUCLEAR STRUCTURE FUNCTIONS

The shadowing of the nuclear structure functions: $R_A(x, Q^2) < 1$ at small $x < 0.1$ can be readily understood in terms of the Gribov-Glauber theory. Consider a two-step process in the nuclear target rest frame. The incoming $q\bar{q}$ dipole first interacts diffractively $\gamma^* N_1 \to (q\bar{q})N_1$ on nucleon N_1 leaving it intact. This is the leading-twist diffractive deep inelastic scattering (DDIS) process which has been measured at HERA to constitute approximately 10% of the DIS cross section at high energies. The $q\bar{q}$ state then interacts inelastically on a downstream nucleon $N_2 : (q\bar{q})N_2 \to X$. The phase of the pomeron-dominated DDIS amplitude is close to imaginary, and the Glauber cut provides another phase i, so that the two-step process has opposite phase and destructively interferes with the one-step DIS process $\gamma * N_2 \to X$ where N_1 acts as an unscattered spectator. The one-step and two-step amplitudes can coherently interfere as long as the momentum transfer to the nucleon N_1 is sufficiently small that it remains in the nuclear target; i.e., the Ioffe length [64] $L_I = 2M\nu/Q^2$ is large compared to the inter-nucleon separation. In effect, the flux reaching the interior nucleons is diminished, thus reducing the number of effective nucleons and $R_A(x, Q^2) < 1$. The Bjorken-scaling diffractive contribution to DIS arises from the rescattering of the struck quark after it is struck (in the parton model frame $q^+ \le 0$), an effect induced by the Wilson line connecting the currents. Thus one cannot attribute DDIS to the physics of the target nucleon computed in isolation [14].

One of the novel features of QCD involving nuclei is the *antishadowing* of the nuclear structure functions as observed in deep inelastic lepton-nucleus scattering. Empirically, one finds $R_A(x, Q^2) \equiv \left(F_{2A}(x, Q^2)/(A/2)F_d(x, Q^2)\right) > 1$ in the domain $0.1 < x < 0.2$; i.e., the measured nuclear structure function (referenced to the deuteron) is larger than the scattering on a set of A independent nucleons. Ivan Schmidt, Jian-Jun Yang, and I [20] have extended the analysis of nuclear shadowing to the shadowing and antishadowing of the electroweak structure functions. We note that there are leading-twist diffractive contributions $\gamma^* N_1 \to (q\bar{q})N_1$ arising from Reggeon exchanges in the t-channel [65]. For example, isospin–non-singlet $C = +$ Reggeons contribute to the difference of proton and neutron structure functions, giving the characteristic Kuti-Weisskopf $F_{2p} - F_{2n} \sim x^{1-\alpha_R(0)} \sim x^{0.5}$ behavior at small x. The x dependence of the structure functions reflects the Regge behavior $\nu^{\alpha_R(0)}$ of the virtual Compton amplitude at fixed Q^2 and $t = 0$. The phase of the diffractive amplitude is determined by analyticity and crossing to be proportional to $-1 + i$ for $\alpha_R = 0.5$, which together with the phase from the Glauber cut, leads to *constructive* interference of the diffractive and nondiffractive multi-step nuclear amplitudes. The nuclear structure function is predicted to be enhanced precisely in the domain $0.1 < x < 0.2$ where antishadowing is empirically observed. The strength of the Reggeon amplitudes is fixed by the Regge fit to the nucleon structure functions, so there is little model dependence. Since quarks of different flavors will couple to different Reggeons; this leads to the remarkable prediction that nuclear antishadowing is not universal; it depends on the quantum numbers of the struck quark. This picture implies substantially different antishadowing for charged and neutral current reactions, thus affecting the extraction of the weak-mixing angle θ_W. The ratio of nuclear to nucleon structure functions is thus process dependent. We have also identified contributions to the nuclear multi-step reactions which arise from odderon exchange and hidden color degrees of freedom in the nuclear wavefunction.

Schienbein et al. [22] have recently given a comprehensive analysis of charged current deep inelastic neutrino-iron scattering, finding significant differences with the nuclear corrections for electron-iron scattering. See Fig. 3. The nuclear effect measured in the NuTeV deep inelastic scattering charged current experiment is distinctly different from the nuclear modification measured at SLAC and NMC in deep inelastic scattering electron and muon scattering. This implies that part of of the anomalous NuTeV result [66] for θ_W could be due to the non-universality of nuclear antishadowing for charged and neutral currents. This effect could also explain the absence of antishadowing observed in Drell-Yan reactions [67, 68].

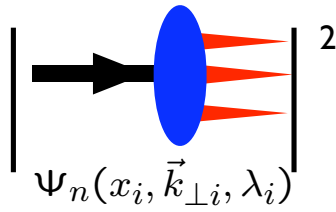A new understanding of nuclear shadowing and antishadowing has emerged based on multi-step coherent reactions
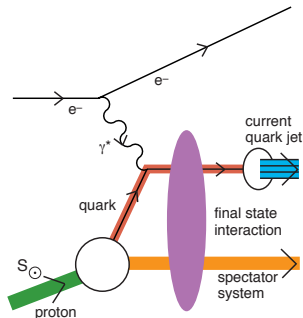
Static	**Dynamic**
• Square of Target LFWFs	Modified by Rescattering: ISI & FSI
• No Wilson Line	Contains Wilson Line, Phases
• Probability Distributions	No Probabilistic Interpretation
• Process-Independent	Process-Dependent - From Collision
• T-even Observables	T-Odd (Sivers, Boer-Mulders, etc.)
• No Shadowing, Anti-Shadowing	Shadowing, Anti-Shadowing, Saturation
• Sum Rules: Momentum and J^z	Sum Rules Not Proven
• DGLAP Evolution; mod. at large x	DGLAP Evolution
• No Diffractive DIS	Hard Pomeron and Odderon Diffractive DIS

FIG. 9: Static versus dynamic structure functions

involving leading twist diffractive reactions [20, 65]. The nuclear shadowing of structure functions is a consequence of the lepton-nucleus collision; it is not an intrinsic property of the nuclear wavefunction. The same analysis shows that antishadowing is *not universal*, but it depends in detail on the flavor of the quark or antiquark constituent [20]. Detailed measurements of the nuclear dependence of individual quark structure functions are thus needed to establish the distinctive phenomenology of shadowing and antishadowing and to make the NuTeV results definitive. A comparison of the nuclear modification in neutrino versus anti-neutrino interactions is clearly important. There are other ways in which this new view of antishadowing can be tested; for example, antishadowing can also depend on the target and beam polarization.

V. DYNAMIC VERSUS STATIC HADRONIC STRUCTURE FUNCTIONS

The nontrivial effects from rescattering and diffraction highlight the need for a fundamental understanding the dynamics of hadrons in QCD at the amplitude level. This is essential for understanding phenomena such as the quantum mechanics of hadron formation, the remarkable effects of initial and final interactions, the origins of diffractive phenomena and single-spin asymmetries, and manifestations of higher-twist semi-exclusive hadron subprocesses. A central tool in these analyses is the light-front wavefunctions of hadrons, the frame-independent eigensolutions of the Heisenberg equation for QCD $H^{LF}|\Psi> = M^2|\Psi>$ quantized at fixed light-front. Given the light-front wavefunctions $\psi_{n/H}(x_i, \vec{k}_{\perp i}, \lambda_i)$, one can compute a large range of exclusive and inclusive hadron observables. For example, the valence, sea-quark and gluon distributions are defined from the squares of the LFWFS summed over all Fock states n. Form factors, exclusive weak transition amplitudes [69] such as $B \to \ell\nu\pi$, and the generalized parton distributions [70]

measured in deeply virtual Compton scattering are (assuming the "handbag" approximation) overlaps of the initial and final LFWFS with $n = n'$ and $n = n' + 2$.

It is thus important to distinguish "static" structure functions which are computed directly from the light-front wavefunctions of a target hadron from the nonuniversal "dynamic" empirical structure functions which take into account rescattering of the struck quark in deep inelastic lepton scattering. See Fig. 9. The real wavefunctions underlying static structure functions cannot describe diffractive deep inelastic scattering nor single-spin asymmetries, since such phenomena involve the complex phase structure of the $\gamma^* p$ amplitude. One can augment the light-front wavefunctions with a gauge link corresponding to an external field created by the virtual photon $q\bar{q}$ pair current [71, 72], but such a gauge link is process dependent [12], so the resulting augmented wavefunctions are not universal. [14, 71, 73]. The physics of rescattering and nuclear shadowing is not included in the nuclear light-front wavefunctions, and a probabilistic interpretation of the nuclear DIS cross section is precluded.

VI. NOVEL INTRINSIC HEAVY QUARK PHENOMENA

Intrinsic heavy quark distributions are a rigorous feature of QCD, arising from diagrams in which two or more gluons couple the valence quarks to the heavy quarks. The probability for Fock states of a light hadron to have an extra heavy quark pair decreases as $1/m_Q^2$ in non-Abelian gauge theory [24, 26]. The relevant matrix element is the cube of the QCD field strength $G_{\mu\nu}^3$, in contrast to QED where the relevant operator is $F_{\mu\nu}^4$ and the probability of intrinsic heavy leptons in an atomic state is suppressed as $1/m_\ell^4$. The maximum probability occurs at $x_i = m_\perp^i / \sum_{j=1}^n m_\perp^j$ where $m_{\perp i} = \sqrt{k_{\perp i}^2 + m_i^2}$; i.e., when the constituents have minimal invariant mass and equal rapidity. Thus the heaviest constituents have the highest momentum fractions and the highest x_i. Intrinsic charm thus predicts that the charm structure function has support at large x_{bj} in excess of DGLAP extrapolations [23]; this is in agreement with the EMC measurements [25]. Intrinsic charm can also explain the $J/\psi \to \rho\pi$ puzzle [74]. It also affects the extraction of suppressed CKM matrix elements in B decays [75]. The dissociation of the intrinsic charm $|uudc\bar{c} >$ Fock state of the proton can produce a leading heavy quarkonium state at high $x_F = x_c + x_{\bar{c}}$ in $pN \to J/\psi X$ since the c and $\bar{c}$ can readily coalesce into the charmonium state. Since the constituents of a given intrinsic heavy-quark Fock state tend to have the same rapidity, coalescence of multiple partons from the projectile Fock state into charmed hadrons and mesons is also favored. For example, one can produce a leading Λ_c at high x_F and low p_T from the coalescence of the udc constituents of the projectile $|uudc\bar{c} >$ Fock state.

The operator product analysis of the IC matrix element shows that the IC Fock state has a dominant color-octet structure: $|(uud)_{8C}(c\bar{c})_{8C} >$. The color octet $c\bar{c}$ converts to a color singlet by gluon exchange on the front surface of a nuclear target and then coalesces to a J/ψ which interacts weakly through the nuclear volume [28]. Thus the rate for the IC component has $A^{2/3}$ dependence corresponding to the area of the front surface. This is illustrated in fig 10. This forward contribution is in addition to the A^1 contribution derived from the usual perturbative QCD fusion contribution at small x_F. Because of these two components, the cross section violates perturbative QCD factorization for hard inclusive reactions [76]. This is consistent with the two-component cross section for charmonium production observed by the NA3 collaboration at CERN [77] and more recent experiments [78]. The diffractive dissociation of the intrinsic charm Fock state leads to leading charm hadron production and fast charmonium production in agreement with measurements [79]. The hadroproduction cross sections for double-charm Ξ_{cc}^+ baryons at SELEX [80] and the production of J/ψ pairs at NA3 are consistent with the diffractive dissociation and coalescence of double IC Fock states [81]. These observations provide compelling evidence for the diffractive dissociation of complex off-shell Fock states of the projectile and contradict the traditional view that sea quarks and gluons are always produced perturbatively via DGLAP evolution or gluon splitting. It is also conceivable that the observations [82] of Λ_b at high x_F at the ISR in high energy pp collisions could be due to the dissociation and coalescence of the "intrinsic bottom" $|uudb\bar{b} >$ Fock states of the proton.
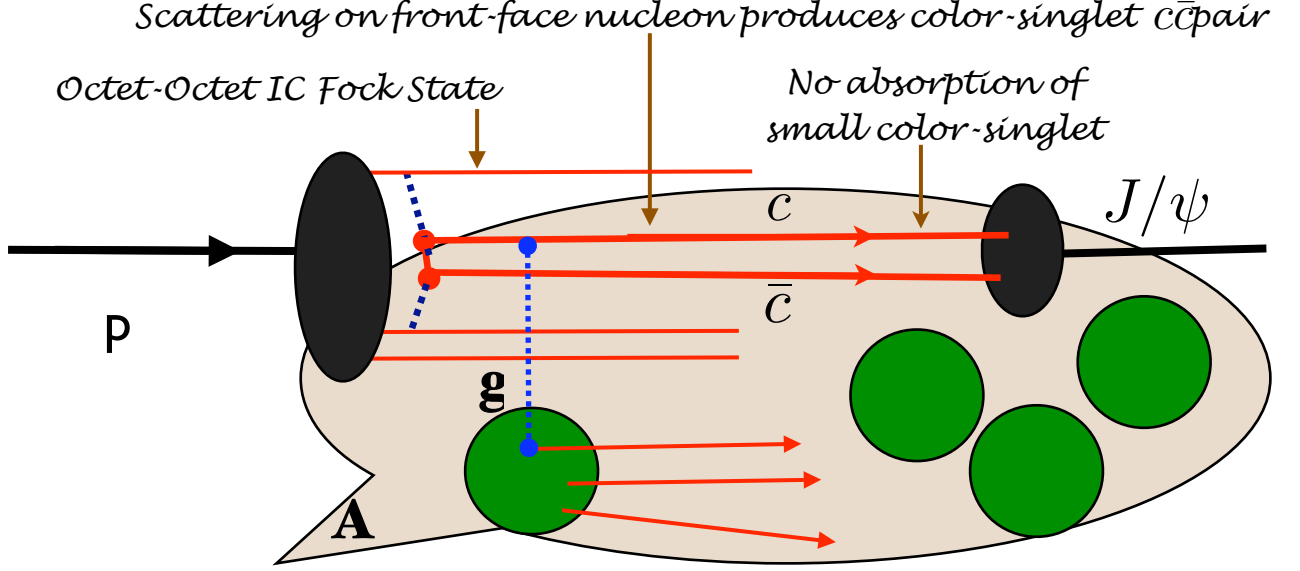
As emphasized by Lai, Tung, and Pumplin [84], there are strong indications that the structure functions used to model charm and bottom quarks in the proton at large x_{bj} have been underestimated, since they ignore intrinsic heavy quark fluctuations of hadron wavefunctions. The anomalous growth of the $p\bar{p} \to \gamma c X$ inclusive cross section observed by D0 collaboration [83] at the Tevatron and shown in Fig. 11 also suggests that the charm distribution has been underestimated at $x > 0.1$, beyond what is included in the CTEQ6.6M pdfs.

The neglect of the intrinsic-heavy quark component in the proton structure function will lead to an incorrect assessment of the gluon distribution at large x if it is assumed that sea quarks always arise from gluon splitting.

The intrinsic charm and bottom distributions at high x in the proton structure functions also lead to novel heavy hadron production processes such as anomalous production of charm and bottom jets at high p_T at the LHC, as well as novel mechanisms for Higgs and Z^0 production at high x_F [28, 85]

It is astonishing that the original EMC experiment which first observed a large signal for charm at large x in

Color-Opaque IC Fock state interacts on nuclear front surface

Scattering on front-face nucleon produces color-singlet $c\bar{c}$ pair

Octet-Octet IC Fock State

No absorption of small color-singlet

c

J/ψ

$\bar{c}$

P

g

A

$$\frac{d\sigma}{dx_F}(pA \rightarrow J/\psi X) = A^{2/3} \times \frac{d\sigma}{dx_F}(pN \rightarrow J/\psi X)$$

FIG. 10: Color-Octet intrinsic charm mechanism for the nuclear dependence of J/ψ production

1983 has never been repeated. It is thus critical for experiments such as COMPASS to definitively establish the phenomenology of the charm structure function at large x_{bj}.

VII.   VACUUM EFFECTS AND LIGHT-FRONT QUANTIZATION

The vacuum in quantum field theories is remarkably simple in light-front quantization because of the restriction $k^+ \geq 0$. For example in QED, vacuum graphs such as $e^+ e^- \gamma$ which are normally associated with a zero-point energy do not arise in the light-front vacuum. In the Higgs theory, the usual Higgs vacuum expectation value is replaced with a $k^+ = 0$ zero mode; [86] however, the resulting phenomenology is identical to the standard analysis.

The usual assumption that non-zero vacuum condensates exist and possess a measurable reality has long been recognized as posing a conundrum for the light-front formulation of QCD. In the light-front formulation of QCD, the ground-state is a structureless Fock space vacuum, in which case it would seem to follow that dynamical chiral symmetry breaking (CSB) is impossible. In fact, as first argued by Casher and Susskind [87], dynamical CSB must be a property of hadron wavefunctions, not of the vacuum. (They used an infinite momentum framework which is equivalent to the front-form.) This thesis has also been explored in a series of recent articles [32, 44, 63].

It is widely held that quark and gluon vacuum condensates have a physical existence, independent of hadrons, as measurable spacetime-independent configurations of QCD's elementary degrees-of-freedom in a hadron-less ground state. However, a non-zero spacetime-independent QCD vacuum condensate poses a critical dilemma for gravitational interactions, because it would lead to a cosmological constant some 45 orders of magnitude larger than observation.
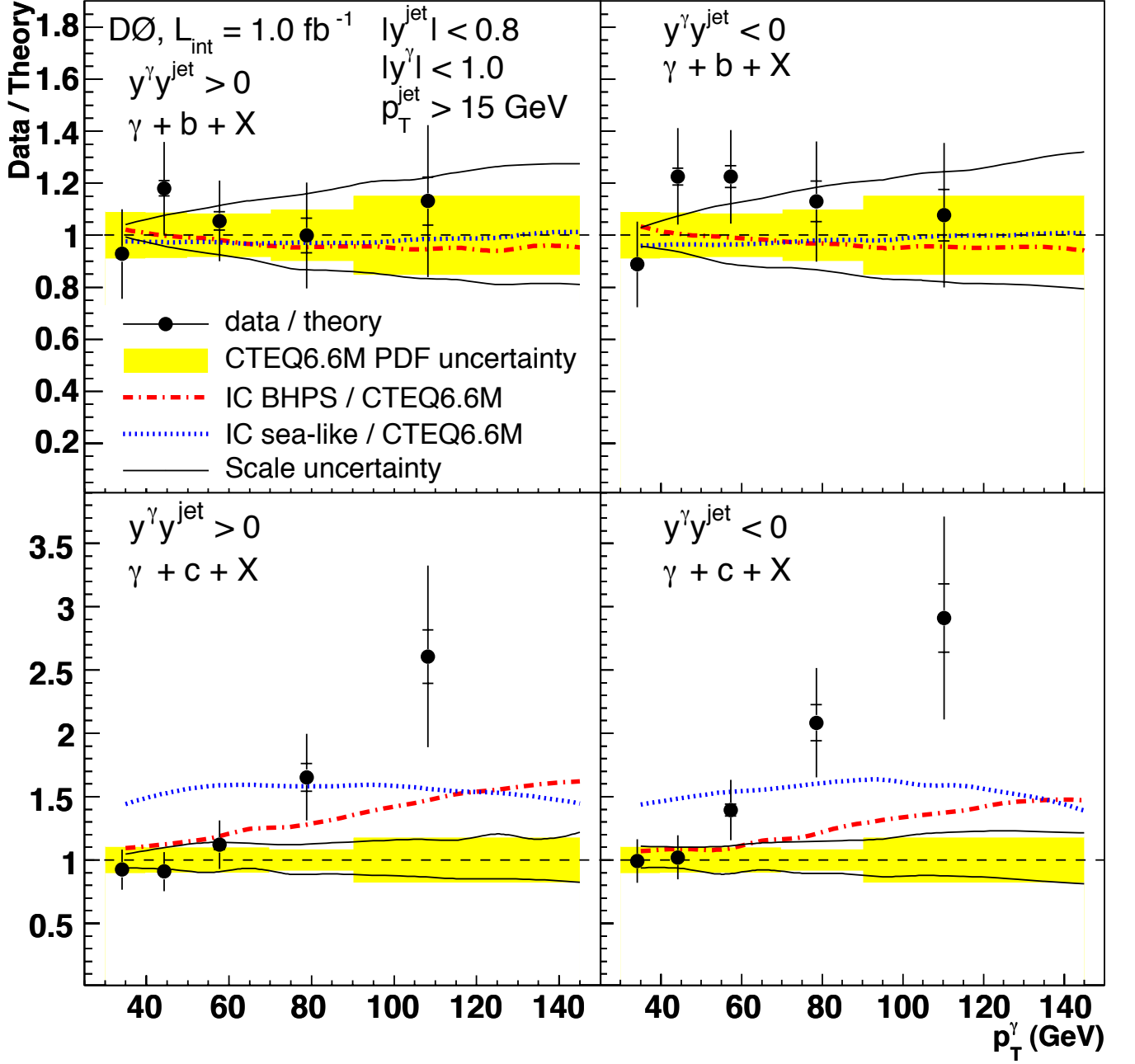
FIG. 11: The data-to-theory ratio of cross sections as a function of the photon transverse momentum for $p\bar{p} \to \gamma b X$ and $p\bar{p} \to \gamma c X$ in the rapidity regions $y^\gamma y^{\text{jet}} > 0$ and $y^\gamma y^{\text{jet}} < 0$. The uncertainties for the data include both statistical (inner line) and full uncertainties (entire error bar). Also shown are the uncertainties on the theoretical pQCD scales and the CTEQ6.6M parameterization of the parton distribution functions (pdfs). The scale uncertainties are shown as dotted lines and the pdf uncertainties by the shaded regions. The ratio of the standard CTEQ6.6M prediction to two models of intrinsic charm is also shown. From the D0 collaboration [83].

As noted in Ref. [32], this conflict is avoided if the strong interaction condensates are properties of the light-front wavefunctions of the hadrons, rather than the hadron-less ground state of QCD.

Conventionally, the quark and gluon condensates are considered to be properties of the QCD vacuum and hence to be constant throughout spacetime. A new perspective on the nature of QCD condensates $\langle \bar{q}q \rangle$ and $\langle G_{\mu\nu}G^{\mu\nu} \rangle$, particularly where they have spatial and temporal support, has recently been presented. [32, 33, 63, 88, 89] The spatial support of condensates is restricted to the interior of hadrons, since condensates in QCD arise due to the

interactions of quarks and gluons which are confined within hadrons. For example, consider a meson consisting of a light quark q bound to a heavy antiquark, such as a B meson. One can analyze the propagation of the light q in the background field of the heavy $\bar{b}$ quark. Solving the Dyson-Schwinger equation for the light quark one obtains a nonzero dynamical mass and evidently a nonzero value of the condensate $\langle \bar{q}q \rangle$. But this is not a true vacuum expectation value; in fact, it is the matrix element of the operator $\bar{q}q$ in the background field of the $\bar{b}$ quark.

The change in the (dynamical) mass of the light quark in a bound state is somewhat reminiscent of the energy shift of an electron in the Lamb shift, in that both are consequences of the fermion being in a bound state rather than propagating freely. It is clearly important to use the equations of motion for confined quarks and gluon fields when analyzing current correlators in QCD, not free propagators, as has often been done in traditional analyses. Since the distance between the quark and antiquark cannot become arbitrarily large, one cannot create a quark condensate which has uniform extent throughout the universe. Thus in a fully self-consistent treatment of a QCD bound state, the condensate phenomenon occurs in the background field of the $\bar{b}$-quark, whose influence on light-quark propagation is primarily concentrated in the far infrared and whose presence ensures the manifestations of light-quark dressing are gauge invariant.

In the case of the pion, one can show from the Bethe-Salpeter equation that the vacuum quark condensate that appears in the Gell-Mann-Oakes-Renner formula, is, in fact, a chiral-limit value of an 'in-pion' condensate [33, 90]. This condensate is no more a property of the "vacuum" than the pion's chiral-limit leptonic decay constant.

One can connect the Bethe-Salpeter formalism to the light-front formalism, by fixing the light-front time τ. This then leads to the Fock state expansion. In fact, dynamical CSB in the light-front formulation, expressed via 'in-hadron' condensates, can be shown to be connected with sea-quarks derived from higher Fock states. This solution is similar to that discussed in Ref. [87]. Moreover, Ref. [91] establishes the equivalence of all three definitions of the vacuum quark condensate: a constant in the operator product expansion, [92, 93] via the Banks-Casher formula, [94] and the trace of the chiral-limit dressed-quark propagator.

VIII.   CONCLUSIONS

I have reviewed a number of QCD topics where conventional wisdom relevant to hadronic physics at the LHC has been challenged.

For example, the initial-state and final-state interactions of the quarks and gluons entering perturbative QCD hard-scattering subprocesses lead to the breakdown of traditional concepts of factorization and universality at leading twist. These soft-gluon rescattering, which are associated with the Wilson line of the propagating partons, lead to Bjorken-scaling single-spin asymmetries, diffractive deep inelastic scattering, the breakdown of the Lam-Tung leading twist relation in Drell-Yan reactions, as well as nuclear shadowing. Furthermore, the Gribov-Glauber theory applied to the antishadowing domain predicts that nuclear structure functions are not universal, but instead depend on the flavor quantum numbers of each quark and antiquark, thus explaining the anomalous nuclear dependence recently observed in deep-inelastic neutrino scattering.

Surprisingly, isolated hadrons can be produced at large transverse momentum at a significant rate at the LHC directly within a hard higher-twist QCD subprocess, rather than from jet fragmentation. Such "direct" processes can explain the observed deviations from perturbative QCD predictions in measurements of inclusive hadron cross sections at fixed $x_T = 2p_T/\sqrt{s}$, as well as the "baryon anomaly", the anomalously large proton-to-pion ratio seen in high centrality heavy-ion collisions.

The intrinsic charm contribution to the proton structure function at high x can explain the anomalously large rate for high p_T photon plus charm jet events observed by D0 at the Tevatron. Intrinsic charm and bottom distributions also imply anomalously large production of charm and bottom jets at high p_T at the LHC, as well as a novel mechanism for Higgs and Z^0 production at high x_F.

The correspondence between theories in a warped anti-de Sitter space and light-front quantization in physical space-time is very powerful, and leads to much insight into QCD dynamics, including a nonperturbative QCD running coupling and a remarkably accurate relativistic LF Schrodinger equation which reproduces much of light-quark spectroscopy and dynamics, using a soft-wall model of with a positive sign dilaton.

Other novel features of QCD have also been discussed, including the consequences of confinement for quark and gluon condensates and the implications for the QCD contribution to the cosmological constant.

I have also emphasized that setting the renormalization scale of the QCD coupling using the scheme-independent BLM method will greatly improve the precision of QCD predictions, and thus greatly increase the sensitivity of searches for new physics at the LHC.

Acknowledgments

[1] F. Arleo, S. J. Brodsky, D. S. Hwang and A. M. Sickles, Phys. Rev. Lett. **105**, 062002 (2010) [arXiv:0911.4604 [hep-ph]].
[2] F. Arleo, S. J. Brodsky, D. S. Hwang and A. M. Sickles, arXiv:1006.4045 [hep-ph].
[3] S. J. Brodsky and A. Sickles, Phys. Lett. B **668**, 111 (2008) [arXiv:0804.4608 [hep-ph]].
[4] S. S. Adler *et al.* [PHENIX Collaboration], Phys. Rev. Lett. **91**, 172301 (2003) [arXiv:nucl-ex/0305036].
[5] D. W. Sivers, S. J. Brodsky and R. Blankenbecler, Phys. Rept. **23**, 1 (1976).
[6] S. J. Brodsky and M. Rijssenbeek, arXiv:hep-ph/0511178.
[7] J. W. Cronin, H. J. Frisch, M. J. Shochet, J. P. Boymond, P. A. Piroue and R. L. Sumner, Phys. Rev. Lett. **31**, 1426 (1973).
[8] D. Antreasyan, J. W. Cronin, H. J. Frisch, M. J. Shochet, L. Kluberg, P. A. Piroue and R. L. Sumner, Phys. Rev. D **19**, 764 (1979).
[9] R. Blankenbecler, S. J. Brodsky and J. F. Gunion, Phys. Rev. D **12**, 3469 (1975).
[10] J. Collins and J. W. Qiu, Phys. Rev. D **75**, 114014 (2007) [arXiv:0705.2141 [hep-ph]].
[11] S. J. Brodsky, D. S. Hwang and I. Schmidt, Phys. Lett. B **530**, 99 (2002) [arXiv:hep-ph/0201296].
[12] J. C. Collins, Phys. Lett. B **536**, 43 (2002) [arXiv:hep-ph/0204004].
[13] S. J. Brodsky, D. S. Hwang and I. Schmidt, Nucl. Phys. B **642**, 344 (2002) [arXiv:hep-ph/0206259].
[14] S. J. Brodsky, P. Hoyer, N. Marchal, S. Peigne and F. Sannino, Phys. Rev. D **65**, 114025 (2002) [arXiv:hep-ph/0104291].
[15] C. Adloff *et al.* [H1 Collaboration], Z. Phys. C **76**, 613 (1997) [arXiv:hep-ex/9708016].
[16] J. Breitweg *et al.* [ZEUS Collaboration], Eur. Phys. J. C **6**, 43 (1999) [arXiv:hep-ex/9807010].
[17] S. J. Brodsky, B. Pasquini, B. W. Xiao and F. Yuan, Phys. Lett. B **687**, 327 (2010) [arXiv:1001.1163 [hep-ph]].
[18] D. Boer, S. J. Brodsky and D. S. Hwang, Phys. Rev. D **67**, 054003 (2003) [arXiv:hep-ph/0211110].
[19] D. Boer, Phys. Rev. D **60**, 014012 (1999) [arXiv:hep-ph/9902255].
[20] S. J. Brodsky, I. Schmidt and J. J. Yang, Phys. Rev. D **70**, 116003 (2004) [arXiv:hep-ph/0409279].
[21] S. J. Brodsky, Nucl. Phys. A **827**, 327C (2009) [arXiv:0901.0781 [hep-ph]].
[22] I. Schienbein, J. Y. Yu, C. Keppel, J. G. Morfin, F. I. Olness and J. F. Owens, arXiv:0806.0723 [hep-ph].
[23] S. J. Brodsky, P. Hoyer, C. Peterson and N. Sakai, Phys. Lett. B **93**, 451 (1980).
[24] S. J. Brodsky, J. C. Collins, S. D. Ellis, J. F. Gunion and A. H. Mueller, published in *Design and Utilization of the SSC, Snowmass, 1984*: proceedings. Edited by Rene Donaldson and Jorge G. Morfin. Batavia, Ill., Fermilab, 1985. 851p.
[25] B. W. Harris, J. Smith and R. Vogt, Nucl. Phys. B **461**, 181 (1996) [arXiv:hep-ph/9508403].
[26] M. Franz, M. V. Polyakov and K. Goeke, Phys. Rev. D **62**, 074024 (2000) [arXiv:hep-ph/0002240].
[27] S. J. Brodsky and B. Q. Ma, Phys. Lett. B **381**, 317 (1996) [arXiv:hep-ph/9604393].
[28] S. J. Brodsky, B. Kopeliovich, I. Schmidt and J. Soffer, Phys. Rev. D **73**, 113005 (2006) [arXiv:hep-ph/0603238].
[29] S. J. Brodsky, M. S. Gill, M. Melles and J. Rathsman, Phys. Rev. D **58**, 116006 (1998) [arXiv:hep-ph/9801330].
[30] G. Kramer and B. Lampe, Z. Phys. A **339**, 189 (1991).
[31] C. F. Berger *et al.*, arXiv:1009.2338 [hep-ph].
[32] S. J. Brodsky and R. Shrock, arXiv:0905.1151 [hep-th].
[33] S. J. Brodsky, C. D. Roberts, R. Shrock and P. C. Tandy, Phys. Rev. C **82**, 022201 (2010) [arXiv:1005.4610 [nucl-th]].
[34] S. J. Brodsky and B. T. Chertok, Phys. Rev. D **14**, 3003 (1976).
[35] V. A. Matveev and P. Sorba, Lett. Nuovo Cim. **20**, 435 (1977).
[36] S. J. Brodsky, C. R. Ji and G. P. Lepage, Phys. Rev. Lett. **51**, 83 (1983).
[37] R. G. Arnold *et al.*, Phys. Rev. Lett. **35**, 776 (1975).
[38] G. R. Farrar, K. Huleihel and H. y. Zhang, Phys. Rev. Lett. **74**, 650 (1995).
[39] G. F. de Teramond and S. J. Brodsky, Phys. Rev. Lett. **94**, 201601 (2005) [arXiv:hep-th/0501022].
[40] G. F. de Teramond and S. J. Brodsky, Phys. Rev. Lett. **102**, 081601 (2009) [arXiv:0809.4899 [hep-ph]].
[41] S. J. Brodsky and G. F. de Teramond, arXiv:1009.4232 [hep-ph].
[42] J. Polchinski and M. J. Strassler, Phys. Rev. Lett. **88**, 031601 (2002) [arXiv:hep-th/0109174].
[43] S. J. Brodsky, G. F. de Teramond and A. Deur, Phys. Rev. D **81**, 096010 (2010) [arXiv:1002.3948 [hep-ph]].
[44] S. J. Brodsky, G. de Teramond and R. Shrock, AIP Conf. Proc. **1056**, 3 (2008) [arXiv:0807.2484 [hep-ph]].
[45] C. T. Munger, S. J. Brodsky and I. Schmidt, Phys. Rev. D **49**, 3228 (1994).
[46] E. L. Berger and S. J. Brodsky, Phys. Rev. Lett. **42**, 940 (1979).
[47] A. M. Sickles, Nucl. Phys. A **830**, 131C (2009) [arXiv:0907.4921 [nucl-ex]].
[48] S. J. Brodsky and A. H. Mueller, Phys. Lett. B **206**, 685 (1988).
[49] S. J. Brodsky, G. P. Lepage and P. B. Mackenzie, Phys. Rev. D **28**, 228 (1983).

[50] G. Grunberg and A. L. Kataev, Phys. Lett. B **279**, 352 (1992).

[51] S. J. Brodsky, G. T. Gabadadze, A. L. Kataev and H. J. Lu, Phys. Lett. B **372**, 133 (1996) [arXiv:hep-ph/9512367].

[52] A. L. Kataev and S. V. Mikhailov, arXiv:1011.5248 [hep-ph].

[53] R. J. Crewther, Phys. Rev. Lett. **28**, 1421 (1972).

[54] D. J. Broadhurst and A. L. Kataev, Phys. Lett. B **315**, 179 (1993) [arXiv:hep-ph/9308274].

[55] S. J. Brodsky and H. J. Lu, Phys. Rev. D **51**, 3652 (1995) [arXiv:hep-ph/9405218].

[56] S. J. Brodsky, E. Gardi, G. Grunberg and J. Rathsman, Phys. Rev. D **63**, 094017 (2001) [arXiv:hep-ph/0002065].

[57] S. J. Brodsky, V. S. Fadin, V. T. Kim, L. N. Lipatov and G. B. Pivovarov, JETP Lett. **70**, 155 (1999) [arXiv:hep-ph/9901229].

[58] S. J. Brodsky and P. Huet, Phys. Lett. B **417**, 145 (1998) [arXiv:hep-ph/9707543].

[59] M. Binger and S. J. Brodsky, Phys. Rev. D **74**, 054016 (2006) [arXiv:hep-ph/0602199].

[60] H. J. Lu, SLAC-0406, Thesis UMI-93-02249-MC. September, 1992.

[61] S. J. Brodsky, A. H. Hoang, J. H. Kuhn and T. Teubner, Phys. Lett. B **359**, 355 (1995) [arXiv:hep-ph/9508274].

[62] S. J. Brodsky and G. F. de Teramond, Phys. Rev. D **77**, 056007 (2008) [arXiv:0707.3859 [hep-ph]].

[63] S. J. Brodsky and R. Shrock, Phys. Lett. B **666**, 95 (2008) [arXiv:0806.1535 [hep-th]].

[64] B. L. Ioffe, Phys. Lett. B **30**, 123 (1969).

[65] S. J. Brodsky and H. J. Lu, Phys. Rev. Lett. **64**, 1342 (1990).

[66] G. P. Zeller *et al.* [NuTeV Collaboration], Phys. Rev. Lett. **88**, 091802 (2002) [Erratum-ibid. **90**, 239902 (2003)] [arXiv:hep-ex/0110059].

[67] D. M. Alde *et al.*, Phys. Rev. Lett. **64**, 2479 (1990).

[68] S. Peigne, Phys. Rev. D **66**, 114011 (2002) [arXiv:hep-ph/0206138].

[69] S. J. Brodsky and D. S. Hwang, Nucl. Phys. B **543**, 239 (1999) [arXiv:hep-ph/9806358].

[70] S. J. Brodsky, M. Diehl and D. S. Hwang, Nucl. Phys. B **596**, 99 (2001) [arXiv:hep-ph/0009254].

[71] A. V. Belitsky, X. Ji and F. Yuan, Nucl. Phys. B **656**, 165 (2003) [arXiv:hep-ph/0208038].

[72] J. C. Collins and A. Metz, Phys. Rev. Lett. **93**, 252001 (2004) [arXiv:hep-ph/0408249].

[73] J. C. Collins, Acta Phys. Polon. B **34**, 3103 (2003) [arXiv:hep-ph/0304122].

[74] S. J. Brodsky and M. Karliner, Phys. Rev. Lett. **78**, 4682 (1997) [arXiv:hep-ph/9704379].

[75] S. J. Brodsky and S. Gardner, Phys. Rev. D **65**, 054016 (2002) [arXiv:hep-ph/0108121].

[76] P. Hoyer, M. Vanttinen and U. Sukhatme, Phys. Lett. B **246**, 217 (1990).

[77] J. Badier *et al.* [NA3 Collaboration], Phys. Lett. B **104**, 335 (1981).

[78] M. J. Leitch *et al.* [FNAL E866/NuSea collaboration], Phys. Rev. Lett. **84**, 3256 (2000) [arXiv:nucl-ex/9909007].

[79] J. C. Anjos, J. Magnin and G. Herrera, Phys. Lett. B **523**, 29 (2001) [arXiv:hep-ph/0109185].

[80] A. Ocherashvili *et al.* [SELEX Collaboration], Phys. Lett. B **628**, 18 (2005) [arXiv:hep-ex/0406033].

[81] R. Vogt and S. J. Brodsky, Phys. Lett. B **349**, 569 (1995) [arXiv:hep-ph/9503206].

[82] G. Bari *et al.*, Nuovo Cim. A **104**, 1787 (1991).

[83] V. M. Abazov *et al.* [D0 Collaboration], Phys. Rev. Lett. **102**, 192002 (2009) [arXiv:0901.0739 [hep-ex]].

[84] J. Pumplin, H. L. Lai and W. K. Tung, Phys. Rev. D **75**, 054029 (2007) [arXiv:hep-ph/0701220].

[85] S. J. Brodsky, A. S. Goldhaber, B. Z. Kopeliovich and I. Schmidt, Nucl. Phys. B **807**, 334 (2009) [arXiv:0707.4658 [hep-ph]].

[86] P. P. Srivastava and S. J. Brodsky, Phys. Rev. D **66**, 045019 (2002) [arXiv:hep-ph/0202141].

[87] A. Casher and L. Susskind, Phys. Rev. D **9**, 436 (1974).

[88] S. J. Brodsky and R. Shrock, arXiv:0803.2541 [hep-th].

[89] S. J. Brodsky and R. Shrock, arXiv:0803.2554 [hep-th].

[90] P. Maris and C. D. Roberts, Phys. Rev. C **56**, 3369 (1997) [arXiv:nucl-th/9708029].

[91] K. Langfeld, H. Markum, R. Pullirsch, C. D. Roberts and S. M. Schmidt, Phys. Rev. C **67**, 065206 (2003) [arXiv:nucl-th/0301024].

[92] K. D. Lane, Phys. Rev. D **10**, 2605 (1974).

[93] H. D. Politzer, Nucl. Phys. B **117**, 397 (1976).

[94] T. Banks and A. Casher, Nucl. Phys. B **169**, 103 (1980).